ISOSCALING IN STATISTICAL MODELS

M.B. Tsang, R. Donangelo[b], W.A. Friedman[a], C.K. Gelbke, X.D. Liu, W.G. Lynch, W.P. Tan, G. Verde, H.S. Xu*, S. R. Souza[b], C.B. Das[c], S. Das Gupta[c], D. Zhabinsky†

I. Introduction

Recently, isotope yields from the central collisions of $^{112}Sn +^{112} Sn$, $^{112}Sn +^{124} Sn$, $^{124}Sn +^{112} Sn$ and $^{124}Sn +^{124} Sn$ collisions have been measured [1]. The ratio of isotope yields from two different reactions, 1 and 2, $R_{21}(N,Z) = Y_2(N,Z)/Y_1(N,Z)$, is found to exhibit an exponential relationship as a function of the isotope neutron number N, and proton number, Z [1, 2].

$$R_{21}(N,Z) = Y_2(N,Z)/Y_1(N,Z) = C{\cdot}exp(\alpha{\cdot}N + \beta{\cdot}Z) \tag{1}$$

where C is an overall normalization factor, α and β are empirical parameters.

Equation (1) can be derived from the primary isotope yields assuming that at breakup the system may be approximated by an infinite equilibrated system and employing the Grand Canonical Ensemble. In this case, predictions for the observed isotopic yield from reaction i are governed by both the neutron and proton chemical potentials, μ_{in} and μ_{ip} and the temperature T, plus the individual binding energies, $B(N,Z)$, of the various isotopes [3, 4]

$$Y_i(N,Z) = F_i(N,Z)exp(B(N,Z)/T)exp(N\mu_{in}/T + Z\mu_{ip}/T) \tag{2}$$

The factor $F_i(N,Z)$ includes information about the secondary decay from both particle stable and particle unstable states to the final ground state yields. If the main difference between system 1 and 2 is the isospin [1, 3, 4], then the binding energy terms in Eq. (2) cancel out in the ratio of $Y_2(N,Z)/Y_1(N,Z)$. If one further assumes that the influence of secondary decay on the yield of a specific isotope is similar for the two reactions, i.e. $F_1(N,Z)\approx F_2(N,Z)$, then Equation (1) is obtained, $\hat{\rho}_n = exp(\Delta\mu_n/T) = exp(\alpha)$ and $\hat{\rho}_p = exp(\Delta\mu_p/T) = exp(\beta)$ are the relative ratios of the free neutron and free proton densities in the two systems, where $\Delta\mu_n$ and $\Delta\mu_p$ are the differences in the neutron and proton chemical potentials. The empirical observation that this fugacity dependence is respected suggests that the effect of sequential decays on $R_{21}(N,Z)$ is small and that $R_{21}(N,Z)$ reflects the properties of the primary source [1]. If true, $R_{21}(N,Z)$ may be an important and robust observable. Furthermore, Eq. (1) allows one to extrapolate isotope yields over a wide range of the reacting systems from the measurements of a few selected isotopes [2].

Since the Grand Canonical limit is strictly valid only for statistical fragment production in an infinite dilute equilibrated system, it is important to study the validity of the scaling behavior of Eq. (1) with realistic models. In this paper, we demonstrate that the isoscaling property of Eq. (1) is also predicted by three additional statistical models, the microcanonical and canonical Statistical Multifragmentation Models as well as the Expanding Emission Source (EES) model. In all three models, isoscaling is affected only slightly by sequential decays, and α and β are mainly sensitive to the proton to neutron composition of the emitting source. In a future paper, we will discuss predictions of non-equilibrium transport models such as the Boltzmann-Nordheim-Vlasov [5] and Antisymmetrized Molecular Dynamics models [6].

II. Microcanonical Statistical Multifragmentation model

To explore the effect of secondary decays on $R_{21}(N,Z)$, we first employ a detailed sequential decay simulation to de-excite primary fragments created in the microcanonical statistical multifragmentation model [7]. Such models have been used successfully to describe fragment multiplicity distributions, charge distributions,

mean kinetic energies, and mean transverse energies of the emitted particles from multifragmentation processes [8, 9]. However, the most commonly used Statistical Multifragmentation Model (SMM) [10, 11] contains only a schematic treatment of the sequential decays of excited fragments and does not include much of the nuclear structure information needed to describe the secondary decay of hot primary fragments. A new improved sequential decay algorithm [7] has been developed to address the secondary decay problem. Each decay from the initial excited fragment is calculated using tabulated branching ratios when available [12], or by using the Hauser-Feshbach formalism [13], when such information is unavailable. Aside from incorporating empirical information on the binding energies of the nuclei, the new algorithm includes accurate structural information such as the discrete bound states and resonant states for nuclei up to Z=15 [7, 14]. This new sequential decay algorithm is coupled to the SMM code of ref. [15], which was chosen mainly for the ease of incorporating the sequential decays of the primary fragments. This newly modified SMM code is referred as SMM-MSU in this article. The physics results should be similar if other SMM codes are used. However, it is worthwhile to note that this SMM code samples the multifragment phase space according to the procedure of Ref. [15] and not according to the Monte Carlo event generation procedure of Refs. [10, 11]. This allows the calculation of low fragment yields of the neutron or proton rich isotopes more precisely.

To examine the effects of secondary decay, the predicted carbon isotope distributions from SMM-MSU are shown in Fig. 1. The primary distributions from a source of A=186, N/Z=1.48 are shown as open points joined by a dashed line while the final distributions after secondary decay are shown as closed circles joined by a solid line in the top panel. Typically, the error bars are smaller than the size of the symbols for most isotopes except the very neutron or proton rich ones. The primary distributions are wide and spread over a large range of neutron-rich nuclei and peak around ^{14}C. After sequential decays, the distributions are much narrower and peaked near ^{12}C, more in agreement with experimental observation. Such narrowing of isotope distributions due to sequential decays has been well established [7, 16, 17, 18].

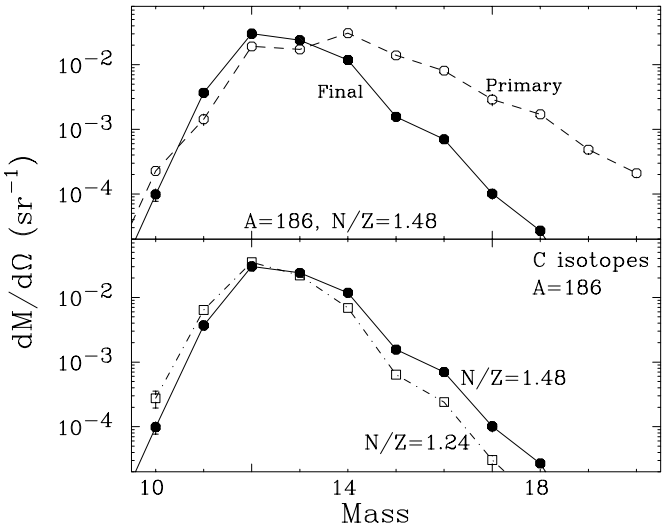

Figure 1: Differential multiplicities at $\theta_{CM} = 90^o$ for carbon isotopes as a function of the mass number of the isotope. Top panel: primary yields are denoted by open points connected by the dashed lines while the solid points joined by solid lines denote the yield after sequential decays (see text for details). Bottom panel: Final Carbon isotope yields for two systems with different isospin asymmetries, closed circles for δ=0.194, N/Z=1.48 and open squares for δ=0.107, N/Z=1.24. The source size is kept constant at A=$N + Z$=186.

It has been suggested in Ref. [19] that the isotope distributions are sensitive to the proton and neutron composition of the sources from which the fragments are emitted. To explore this issue, we eliminate the size effect by changing the charge of the emitting source but keeping the size constant, i.e. A=186. The carbon

isotope distributions after secondary decay with N/Z=1.48 (closed circles) and N/Z=1.24 (open squares) are compared in the bottom panel of Fig. 1. As expected, more neutron rich isotopes (A>12) are produced from the neutron richer system, while the opposite is true for the proton-rich isotope yields. This trend is consistent with experimental observation [1]. It suggests that isotope yield distributions can be used to study properties that reflect the isospin asymmetry of the emitting sources.

Fig. 1 illustrates an important point that the isospin effects on isotope yields are much reduced by sequential decays. The differences between the final isotope yields from two systems with different isospin asymmetry are much less than those between primary isotope distributions. It is thus important to search for observables such as relative isotope ratios, which cancel out some of the effects of sequential decays, binding energy etc. on isotope productions.

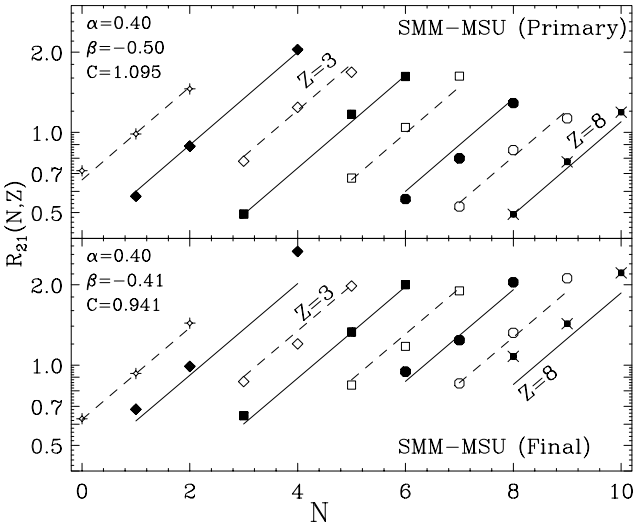

Figure 2: Predicted (symbols) relative isotope ratios, $R_{21}(N,Z)$, of Eq. (1) for the two systems, A_1=168, Z_1=75 and A_2=186, Z_2=75 using the SMM-MSU code [13,20] as a function of N obtained from the primary isotope yields (upper panel) and the final yields after sequential decays (lower panel). Solid and dashed lines are best fits to Equation (1) using the predicted ratios.

In Fig. 2, the relative isotope ratios $R_{21}(N,Z)$ are plotted, as a function of N for the primary (top panel) and secondary isotope (bottom panel) yields predicted by the SMM-MSU model. We choose A_1=168 and Z_1=75 (N_1/Z_1=1.24, δ_1 =0.107) and A_2=186, Z_2=75 (N_2/Z_2=1.48, δ_2=0.194) for sources 1 and 2 where A_i and Z_i are the mass and charge number of source i. The open symbols represent $R_{21}(N,Z)$ of odd-Z elements while the closed symbols are predicted ratios for the even-Z elements. The ratios of both primary and secondary fragments closely follow the trend described by Eq. (1); isotopes of the same Z, plotted with the same symbol, lie along lines with similar slope in the semi-log plots. For comparison, the solid and dashed lines correspond to the calculations using the best-fit values of α, β and C of Eq. (1) to the predicted ratios. Since more neutron-rich isotopes are produced from the neutron-rich system, the slopes of these lines are positive. More importantly, the slopes are similar for all elements before and after sequential decay.

For oxygen isotopes, the agreement between predicted ratios after sequential decays and the best fit lines is not very good. This discrepancy may be an artifact from the sequential decay algorithm used. The current secondary decay code which has structural information for nuclei up to $Z = 15$ may not be reliable for secondary yields with large Z. The effect of incomplete structural information on sequential decays is illustrated in Fig. 3. The histograms represent calculations for the carbon (upper panel) and oxygen (lower panel) isotope distributions which use the Hauser Feshbach decay formalism [13] and take into account all the experimental structural information up to $Z = 15$. Closed points joined by dashed lines are the isotope distributions when

the Hauser Feshbach formalism is used with the experimental structural information up to $Z = 10$ only [7]. In both cases, decays of heavier fragments not calculated via the Hauser Feshbach approach are calculated with the Weisskopf formalism and liquid-drop binding energies [20, 21]. While the yields for the carbon isotopes are similar with both decay tables, the yields for the neutron rich oxygen isotopes are quite different. Sequential decay calculations with more complete structure information predict more yields for neutron-rich oxygen isotopes. This indicates that sequential charged particle decay plays an important role in producing neutron-rich isotopes and that structure information is relevant to such calculations.

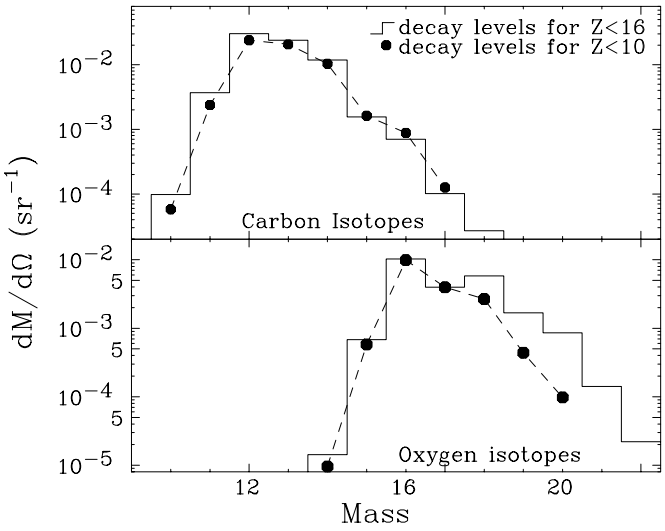

Figure 3: Differential multiplicities at $\theta_{CM} = 90^o$ for carbon (top panel) and oxygen (bottom panel) isotopes as a function of the mass number. Closed points are predictions if the sequential decay information from Ref. [13] where the sequential decay table truncates at Z=13, is used. Histograms are predictions when the structure information in Ref [13] is extended to Z=15 [20].

III. Expanding Emitting Source model

The Expanding Evaporating Source (EES) model [22] provides an alternative description of multifragmentation. The EES model utilizes a rate equation formula similar to the evaporation formalism. The emission rate of fragments with $3 \leq Z \leq 20$ is enhanced when the residue expands to sub-saturation density. Within the context of this model, the neutron scaling parameter, α can be described analytically and provide some physics insight regarding the symmetry energy [2].

To understand the origin of isoscaling in the EES approach, we must examine the EES fragment emission rate. Similar to the formalism of Friedman and Lynch [23], statistical decay rates in the EES model are derived from detailed balance following the Weisskopf model [20]. When the relative rates are dominated by emission within a particular window of source-mass or source-temperature, the relative yields are directly related to the instantaneous rates

$$dn(N,Z)/dt \propto T^2 \cdot exp(-V_c/T + N \cdot f_n^*/T + Z \cdot f_p^*/T - B/T) \tag{3}$$

where V_c gives the Coulomb barrier, and the terms f_n^* and f_p^* represent the excitation contributions to the free energy per neutron and proton, respectively. The factor $B = BE(N_i, Z_i) - BE(N_i - N, Z_i - Z) - BE(N, Z)$ reflects the separation energy associated with the removal of the isotope (N,Z) from the parent nucleus, here denoted by the subscript "i".

When constructing $R_{21}(N, Z)$, some terms, such as the binding energy of the emitted isotope, BE(N,Z), cancel out in the ratio, simplifying the analysis of the dependence of $R_{21}(N, Z)$ on N and Z. To use what

remains of the N and Z dependence of the separation energy term B, we expand the differences in the binding energies of the residues with neutron number $N_i - N$ and proton number $Z_i - Z$ in a Taylor series as follows:

$$BE(N_2 - N, Z_2 - Z) - BE(N_1 - N, Z_1 - Z) \approx a{\cdot}N + b{\cdot}Z + c{\cdot}N^2 + d{\cdot}Z^2 + e{\cdot}N{\cdot}Z \tag{4}$$

Where a, b, c, d and e are coefficients of the Taylor series. Empirically, the coefficients, c, d, and e of the higher terms in N^2, Z^2 and $N{\cdot}Z$ are surprisingly small. One can approximate the binding energy difference with the two leading order terms that depend on the difference in the proton and neutron separation energies between the two systems, 1 and 2 i.e. $a = -\Delta s_p$, $b = -\Delta s_n$. Assuming for simplicity that the residues for systems 1 and 2 have the same charge, $R_{21}(N, Z)$ can be written as follows:

$$R_{21}(N, Z) \propto exp[(-\Delta s_n + \Delta f_n^*){\cdot}N + (-\Delta s_p + \Delta f_p^* + e\Delta\Phi(Z_i - Z)){\cdot}Z/T] \tag{5}$$

where $\Phi(Z)$ is the difference between electrostatic potential at the surface of residue 1 and residue 2. Δf^* is the differences in free energy for the two systems. Aside from the second order term from the electrostatic potential, which is small for the decay of large nuclei, all terms in the exponent of Eq. 5 are proportional to either N or Z, resembling Eq. (1). The corresponding scaling parameters α and β are functions of the separation energies, the Coulomb potential and small contributions from the free excitation energies.

In general, the contribution from free energy is found to be much smaller than the contribution from the separation energy. This is particularly true for systems of comparable mass and energy but different N/Z ratio. Moreover, the volume, surface, and Coulomb contributions to the separation energy largely cancel if the masses of the parent nuclei are similar, leaving the difference in symmetry energies alone as the dominant contribution to Δs_n. The symmetry energy takes the form:

$$E_{sym} = C_{sym}(N - Z)^2/A = C_{sym}(A - 2Z)^2/A \tag{6}$$

The change in neutron separation energy between the two systems can be approximately obtained by taking the derivatives in Eq. (6) with respect to N

$$\alpha = -\Delta s_n/T \approx 4C_{sym}[(Z_1/A_1)^2 - (Z_2/A_2)^2]/T \tag{7}$$

In terms of the isospin asymmetry parameter, $\delta_i = \frac{N_i - Z_i}{A_i}$,

$$\alpha = 2{\cdot}C_{sym}{\cdot}\Delta\delta\left(1 - \bar{\delta}\right) \tag{8}$$

where $\Delta\delta = \delta_2 - \delta_1$, and $\bar{\delta} = \frac{\delta_1 + \delta_2}{2}$. Eq. (8) shows how α depends on the asymmetries δ_i of the two systems. This dependence leads to a non-linear dependence on N_2 and Z_2 and a linear relationship between $(Z_2/A_2)^2$ and α for a fixed system 1. In the EES model, the symmetry energy term, C_{sym}, which takes the liquid drop value of 23.4 MeV [21], must be extrapolated to sub-saturation density as the system expands, i.e., C_{sym} is density dependent. Measurements of $R_{21}(N, Z)$ may thus probe the density dependence of the symmetry energy as discussed in Ref. [2, 14].

IV. Canonical Model

To explore the relationship between the neutron and proton composition of the source (Z_2/A_2) and α in the statistical fragmentation models, we must perform calculations with different sources.

For these studies we use the statistical multifragmentation model (SMM-McGill) [19] that adopts recursive techniques to shorten the time needed for a canonical calculation. We have compared the predictions of this canonical approach to the microcanical model of ref. [7]; the two approaches provide similar predictions for the observables presented below. There are also similarities between these two approaches and the predictions of the Grand Canonical ensemble [18, 24].

We kept our reference system (reaction 1) fixed at A_1=168, Z_1=75 and performed calculations on systems with different (N_2/Z_2) values. The results are shown in Fig. 3. Four groups of calculations are performed by either keeping source size constant at A_2=186 (solid circles), or A_2=124 (open circles) or by keeping the charge of the source constant at Z_2=75 (closed squares) or Z_2=50 (open squares). All four systems with different source sizes lie along one curve. Thus, the slope parameters α and therefore the isotope distributions are not sensitive to the system sizes and charges. They are mainly dependent on the isospin composition, (N_2/Z_2) or equivalently on the isospin asymmetry $\delta_2 = (N_2/Z_2 - 1)/(N_2/Z_2 + 1)$, of system two. The experimental linear relationship between $\hat{\rho}_n$ and (N_2/Z_2) is observed approximately for (N_2/Z_2) >1.2. For $(N_2/Z_2) < 1.2$, there is a concave curvature in $\hat{\rho}_n$ which is especially noticeable at small N_2/Z_2. Instead of a linear relationship, the points in Fig. 4 are better described by the solid curve of the form,

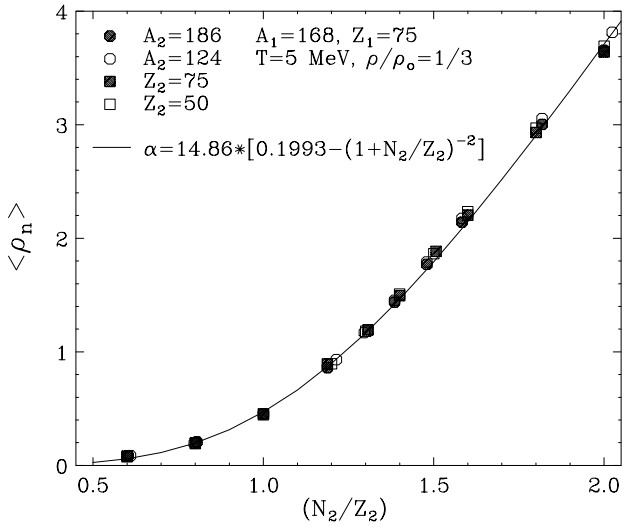

Figure 4: The relative free n-density, $\hat{\rho}_n = exp(\alpha)$, is plotted as a function of the N_2/Z_2 ratio of the source. A linear relationship is observed over the range of N_2/Z_2=1.24 and 1.48, similar to the experimental results. However, over a wider range, the dependence of $\hat{\rho}_n$ on N_2/Z_2 is not linear and the trend is well described by Eq. (9). See text for details.

$$\alpha = 14.86[0.1993 - (1 + N_2/Z_2)^{-2}] = 14.86[0.1993 - (Z_2/A_2)^2] \tag{9}$$

Comparing this formula to Eq. (7), we see that relationship between α and $(Z_2/A_2)^2$ predicted by the EES model, is evident in the SMM calculations. If T is taken to be 5 MeV, Eqs. 7 and 9, give a value of C_{sym}=18.6 MeV as compared to the liquid drop model value, C_{sym} =23.4 MeV [21]. Such dependence probably signals the importance of the symmetry energy as the dominant contribution to α in the SMM model. Indeed, if the asymmetry terms to the binding energies of the nuclei are turned off in the SMM and EES calculations, the isoscaling behavior observed in Fig. 2 disappears.

This work is supported by the National Science Foundation under Grant No. PHY-95-28844, PHY-96-05140, INT-9908727 and contract No. 41.96.0886.00 of MCT/FINEP/CNPq (PRONEX).

a: Department of Physics, University of Wisconsin, Madison, WI 53706
b: Instituto de Fsica, Universidade Federal do Rio de Janeiro, Cidade Universitria, CP 68528, 21945-970 Rio de Janeiro, Brazil
c: Physics Department, McGill University, 3600 University Street, Montreal, Canada H3A 2T8
*: On leave from the Institute of Modern Physics, Lanzhou, China
†: Research Experience for Undergraduates at Michigan State University, 2000

References

1. H.S. Xu, M.B. Tsang, T.X. Liu, X.D. Liu, W.G. Lynch, W.P. Tan A. Vander Molen, G. Verde, A. Wagner, H.F. Xi, and C.K. Gelbke, L. Beaulieu, B. Davin, Y. Larochelle, T. Lefort, R.T. de Souza, R. Yanez, V.E. Viola, R.J. Charity, L.G. Sobotka; Phys. Rev. Lett. 85, 716 (2000).
2. M.B. Tsang, W.A. Friedman, C.K. Gelbke, W.G. Lynch, G. Verde, and H.S. Xu Phys. Rev. Lett. 86, 5023 (2001).
3. S. Albergo S. Costa, E. Costanzo, A. Rubbino, Nuovo Cimento A 89, 1 (1985).
4. J. Randrup and S.E. Koonin, Nucl. Phys. A 356, 223 (1981).
5. A.B. Larionov, A.S. Botvina, M. Colonna, and M Di Toro, Nucl. Phys. A658, 375 (1999) and M. Colonna, private communications.
6. Yoshiharu Tosaka, Akira Ono, and Hisashi Horiuchi, Phys. Rev. C 60, 064613 (1999) and A. Ono, private communications
7. S.R. Souza, W.P. Tan, R. Donangelo, C.K. Gelbke, W.G. Lynch, and M.B. Tsang, Phys. Rev. C62, 064607 (2000).
8. M. D'Agostino, A.S. Botvina, P. M. Milazzo, M. Bruno, G. J. Kunde, D.R. Bowman, L. Celano, N. Colonna, J. D. Dinius, A. Ferrero, M. L. Fiandri, C. K. Gelbke, T. Glasmacher, F. Gramegna, D. O. Handzy, D. Horn, W. C. Hsi, M. Huang, I. Iori, M. A. Lisa, W. G. Lynch, L. Manduci, G. V. Margagliotti, P. F. Mastinu, I.N. Mishustin, C. P. Montoya, A. Moroni, G. F. Peaslee, F. Petruzzelli, L. Phair, R. Rui, C. Schwarz, M. B. Tsang, G. Vannini, and C. William, Phys. Lett. B 371, 175 (1996).
9. C. Williams, W. C. Lynch, C. Schwarz, M.B. Tsang, W.C. Hsi, M.J. Huang, D.R. Bowman, J. Dinius, C. K. Gelbke, D.O. Handzy, G.J. Kunde, M.A. Lisa, C.F. Peaslee, L. Phair, A. Botvina, M.C. Lemaire, S.R. Souza, C. Van Buren, R.J. Charity, L.G. Sobotka, U. Lynen, I. Pochodzalla, H. Sann, W. Trautmann, D. Fox, R.T. de Souza, and N. Carlin, Phys. Rev. C55, R2132 (1997).
10. J. P. Bondorf, A.S. Botvina, A.S. Iljinov, I. N. Mishustin, and K. Sneppen, Phys. Rep. 257, 133 (1995)
11. A.S. Botvina, I.N. Mishustin, M. Begemann-Blaich, J. Hubele, G. Imme, I. Iori, P. Kreutz, G. Kunde, W.D. Kunze, V. Lindenstruth, U. Lynen, A. Moroni, W.F.J. Müller, C.A. Oglivie, J. Pochodzalla, G. Raciti, T. Rubehn, H. Sann, A. Schüttauf, W. Seidel, W. Trautmann, and A. Wörner, Nucl. Phys. A584, 737 (1995).
12. F. Ajzenberg-Selove, Nucl. Phys. A392 (1983) 1; A413 (1984) 1; A433 (1985) 1; A449 (1985) 1; A460 (1986) 1.
13. W. Hauser and H. Feshbach, Phys. Rev. 87, 366 (1952).
14. W.P. Tan, B-A. Li, R. Donangelo, C.K. Gelbke, M-J. van Goetherm, X.D. Liu, W.G. Lynch, S. Souza, M.B. Tsang, G. Verde, A. Wagner and N.S. Xu, preprint, MSUCL-1198 (2001) and http://xxx.lanl.gov/abs/nucl-ex/0104017.
15. J.P. Bondorf, R. Donangelo, I.N. Mishustin, C.J. Pethick, H. Schulz, and K. Sneppen, Nucl. Phys. A 443, 321 (1985), J.P. Bondorf, R. Donangelo, I.N. Mishustin, and H. Schulz, Nucl. Phys. A 444, 460 (1985)
16. J. Barrette, P. Braun-Munzinger, C.K. Gelbek, H.L.Harney, H.E. Wegner, B. Zeidman, K.D. Hildenbrand and U. Lynen, Nucl. Phys. A299, 147 (1978).
17. A.S. Botvina, A.S. Iljinov, I.N. Mishustin, J.P. Bondorf, R. Donangelo and K. Sneppen, Nucl. Phys. A475, 663 (1987).
18. Scott Pratt, Wolfgang Bauer, Christopher Morling, and Patrick Underhill, Phys. Rev. C 63, 034608 (2001).
19. A. Majumder and S. Das Gupta, Phys. Rev. C 61, 034603 (2000); Scott Pratt and Subal Das Gupta, Phys. Rev. C 62, 044603 (2000)
20. V. Weisskopf, Phys. Rev, 52, 295 (1937)
21. Aage Bohr and Ben R. Mottelson, Nuclear Structure, (W.A. Benjamin Inc., New York, 1998), Vol II.
22. W.A. Friedman, Phys. Rev. Lett. 60, 2125 (1988); and Phys. Rev. C42, 667 (1990).
23. W.A. Friedman and W.G. Lynch, Phys. Rev. C28, 16 (1983).
24. B. Das, S. Das Gupta, X. D. Liu and M. B. Tsang, nucl-th/0106019 and to be published.